Efficient Near-Infrared Light-Driven Hydrogen Evolution Catalyzed by a Saddle-Distorted Porphyrin as a Photocatalyst

Hiroaki Kotani,[†] Takuya Miyazaki,[†] Emi Aoki,[†] Hayato Sakai,[‡] Taku Hasobe,[‡] Takahiko Kojima*[,†]

†*Department of Chemistry, Faculty of Pure and Applied Sciences, University of Tsukuba, 1-1-1 Tennoudai, Tsukuba, Ibaraki 305-8571, Japan*
‡*Department of Chemistry, Faculty of Science and Technology, Keio University, Yokohama, 223-8522, Japan*
Supporting Information Placeholder

ABSTRACT: Development of near-infrared (NIR) light-induced hydrogen (H_2) evolution system is indispensable to construct a sustainable society to maximize the utilization of solar energy. Here, we report NIR light-driven H_2 evolution catalyzed by a combination of a diprotonated saddle-distorted porphyrin as a photosensitizer and platinum nanoparticles as a H_2-evolving catalyst. The quantum yield at 710 nm was determined to be 17%, which is the highest value among photocatalytic H_2-evolution systems ever reported.

KEY WORDS: *near-infrared (NIR) light, diprotonated saddle-distorted porphyrin, H_2 evolution reactions (HERs), quantum yield, photoinduced electron transfer, photocatalysis*

Hydrogen (H_2) is a promising and clean energy source for fuel cells to reduce the dependence on fossil fuels.[1,2] Therefore, an efficient photocatalytic system capable of H_2 evolution reactions (HERs) should be constructed on the basis of solar energy because H_2 has been industrially manufactured by energy-consuming methods such as steam reforming of natural gas.[2] To this end, extensive efforts have been devoted to developing photocatalytic HER composed of molecular photocatalysts and H_2 evolution catalysts such as metal complexes or Pt nanoparticles (PtNPs).[3-8] The archetypal photocatalysts[9,10] mainly absorb visible lights to proceed photocatalytic HER efficiently, although the sun light contains not only UV-vis lights but also near-infrared (NIR) ones. Thus, the development of NIR light-responsible photocatalysts is indispensable to maximize the utilization of remaining solar energy for HER. However, there are a few limited examples to demonstrate NIR light-driven HER by heterogeneous semiconductors[11,12] or metal complexes[13-16] as photocatalysts, just affording low quantum yields (up to 4%). Among organic photocatalysts, porphyrins are good candidates for NIR light-induced HER owing to their optical and redox properties based on the 18π aromatic macrocyclic structure.[17-19] So far, porphyrins have been employed as NIR light-responsible photosensitizers in photodynamic therapy because light in the NIR range of 650-800 nm can only penetrate tissues effectively.[20] In addition, the absorption bands of porphyrins could be extended (~750 nm) by introducing distortion to the porphyrin core and the following diprotonation.[11] Recently, a diprotonated saddle-distorted dodecaphenylporphyrin (H_4DPP^{2+})[23] has been employed as a photoredox catalyst for photocatalytic oxidation of substrates[24] and oxygen reduction reactions[25] based on the photodynamics and electron-transfer (ET) properties of H_4DPP^{2+}.[26-29] However, organic photocatalysts responsible to NIR lights have yet to be reported, which would open a development of NIR light-driven HER. We report herein a construction of an NIR light-driven H_2 evolution system consisting of $H_4DPP^{2+}(Cl^-)_2$ and PtNPs in the presence of an electron donor (Scheme 1). Evaluation of NIR light-driven HER was performed by a determination of initial rates of HER and quantum yields at the excitation wavelength, respectively.

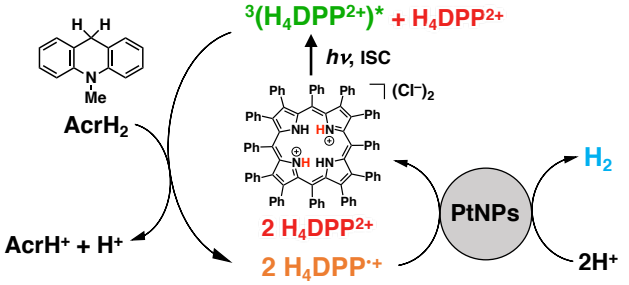

Scheme 1. Schematic Representation of the Approaches for Photocatalytic HER by $H_4DPP^{2+}(Cl^-)_2$.

Poly(vinylpyrrolidone)-protected PtNPs were synthesized according to the literature (see Experimental Section in the Supporting Information (SI)).[30] The average size of PtNPs was determined to be 3.8 ± 0.8 nm by transmission electron microscopy (TEM) measurements together with dynamic light scattering (DLS) measurements (3.8 ± 0.5 nm) as shown in Figure S1. It should be noted that the best size of PtNPs for a HER catalyst has been reported to be around 4 nm.[31,32] Then, an elemental analysis of PtNPs afforded the weight ratio between PtNPs and poly(vinylpyrrolidone), resulting the determination of Pt contents (0.16 mg mL^{-1}) in the stock solution of PtNPs (see Experimental Section in SI).

We performed NIR light-driven HER under catalytic conditions by employing $H_4DPP^{2+}(Cl^-)_2$ as a photocatalyst[33] together with PtNPs as a H_2 evolution catalyst and 10-methyl-9,10-dihydroacridine ($AcrH_2$) as a two-electron donor in the presence of *p*-toluenesulfonic acid (TsOH) as a proton source. Note that no interaction was detected between H_4DPP^{2+} and PtNPs in the ground state, since no spectral change was observed in the UV-vis spectrum of H_4DPP^{2+} upon addition of PtNPs (Figure S2). Photoirradiation (λ = 710 nm) to a methanol (MeOH) and acetonitrile (MeCN) mixed solution (1:1 v/v) containing H_4DPP^{2+}, PtNPs, $AcrH_2$, and TsOH under Ar resulted in the efficient evolution of H_2 detected by gas chromatography (GC). Several control experiments were performed in the absence of each component one by one to confirm the necessity (Figure S3), resulting all components are essential for promoting photocatalytic HER. In order to confirm the stoichiometry of HER, the amounts of products were quantified by UV-vis measurements during photocatalytic HER as shown in Figure 1a. An absorption band at 357 nm assigned to the oxidized product of $AcrH_2$ ($AcrH^+$) increased, although the absorption bands at 485 nm and 706 nm of H_4DPP^{2+} were intact, indicating the robustness of H_4DPP^{2+} under the catalytic conditions. The time profile of H_2 evolution is almost consistent with that of $AcrH^+$ formation (Figure 1b), which indicates that photocatalytic HER proceed almost stoichiometrically by consuming $AcrH_2$ as a two-electron source (eq 1).

$$AcrH_2 + H^+ \xrightarrow[MeOH/MeCN = 1:1\ (v/v)]{h\nu,\ H_4DPP^{2+},\ PtNPs} AcrH^+ + H_2 \quad (1)$$

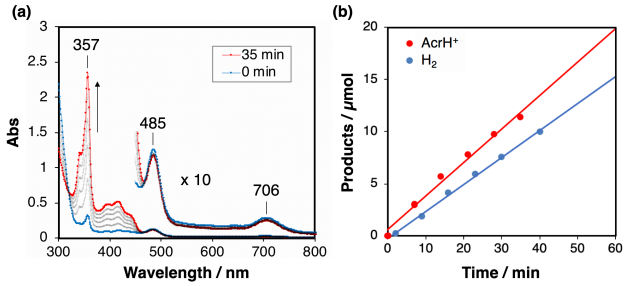

Figure 1. (a) UV-vis spectral changes in photocatalytic HER (λ = 710 nm) observed after a 20-fold dilution. Conditions for HER: $[H_4DPP^{2+}]$ = 10 μM, [TsOH] = 30 mM, [PtNPs] = 0.15 mg mL^{-1}, $[AcrH_2]$ = 5 mM in a MeOH/MeCN mixed solution (4 mL, 1:1 v/v) under Ar at 298 K. (b) Time profiles of product amounts for $AcrH^+$ and H_2.

Next, we investigated dependence of HER on the concentrations of PtNPs, $AcrH_2$, acids, and H_4DPP^{2+} to optimize the photocatalytic conditions. When the amount of evolved H_2 was plotted against photoirradiation time, the initial rate of HER (v_H, μmol min^{-1}) was determined on the basis of the initial slope of the plots (Figure S4). The dependence of v_H on the concentration of $AcrH_2$ ($[AcrH_2]$) showed saturation behavior (Figure 2a), suggesting that $AcrH_2$ should be involved in a rate-determining step in

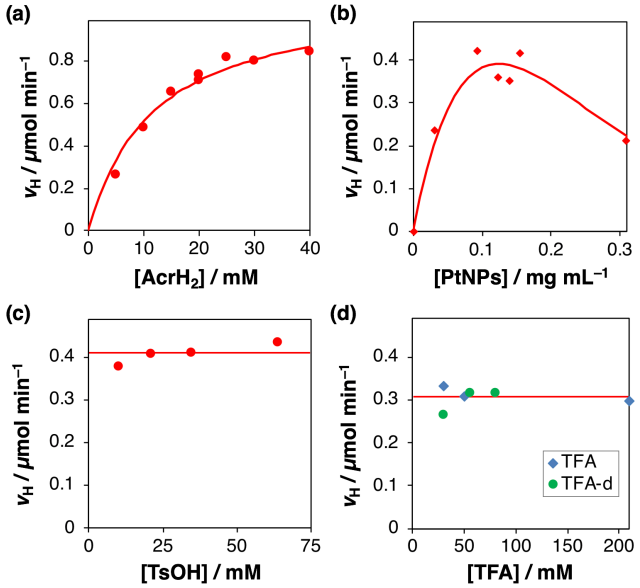

Figure 2. Plots of v_H vs (a) $[AcrH_2]$ in the presence of TsOH (30 mM) and PtNPs (0.15 mg mL^{-1}), (b) [PtNPs] in the presence of TsOH (30 mM) and $AcrH_2$ (10 mM), (c) [TsOH] and (d) [TFA] in the presence of PtNPs (0.15 mg mL^{-1}) and $AcrH_2$ (10 mM), under photocatalytic HER conditions (λ = 710 nm) in a MeOH/MeCN mixed solution (4 mL, 1:1 v/v) containing H_4DPP^{2+} (10 μM) under Ar at 298 K.

photocatalytic HER as discussed later. As for [PtNPs], a bell-shaped dependence of v_H on [PtNPs] was observed within 0.30 mg mL^{-1}, showing the highest performance in the range of 0.10-0.16 mg mL^{-1}, as shown in Figure 2b. In contrast, no dependence of v_H on [TsOH] was observed even in the case of a weaker acid such as trifluoroacetic acid (TFA)[33] (Figure 2c,d), indicating no correlation with the apparent proton concentration ($[H^+]$) in the mixed solvent. Additionally, no kinetic isotope effect (KIE = v_H/v_D = 1) was observed,[31] when deuterated TFA (TFA-*d*) was employed as depicted in Figure 2d. Judging from no dependence of v_H on acid concentrations and the lack of KIE, the formation of a putative Pt-H species between a Pt atom of reduced PtNP and a proton on the surface of PtNPs is not involved in the rate-determining step in contrast to the reported photocatalytic HER by using the same size of PtNPs.[31] When we increased the concentration of H_4DPP^{2+}, the v_H value increased slightly with showing saturation behavior because the amount of absorbed photons at 710 nm increased with increasing $[H_4DPP^{2+}]$ owing to the elevated absorbance at 710 nm (Figure S5). In terms of quantum yields (Φ) based on the absorbed photons, no dependence of the Φ values on $[H_4DPP^{2+}]$ was observed, indicating H_4DPP^{2+} acts as a photosensitizer rather than a H_2-evolving catalyst.

Under the optimized photocatalytic HER conditions, a turnover number (TON) of NIR light-driven HER based on $[H_4DPP^{2+}]$ was reached 1500 at 3 hours with the 72% yield of H_2 based on $[AcrH_2]$ as shown in Figure 3. In order to interpret the saturation behavior of v_H vs photoirradiation time, repeated photocatalytic HER experiments were

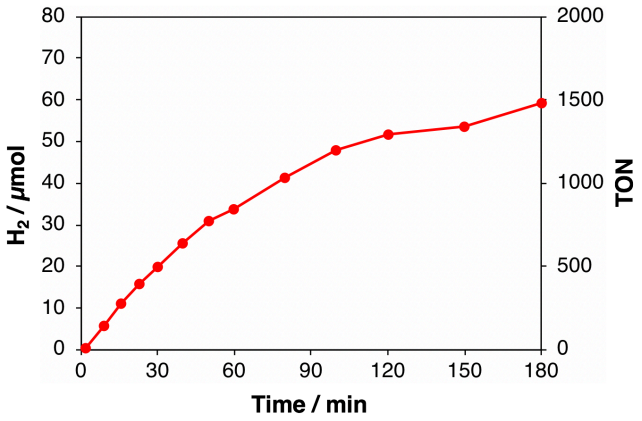

Figure 3. A time course of H_2 evolution under photoirradiation ($\lambda = 710$ nm) in a MeOH/MeCN mixed solution (4 mL, 1:1 v/v) containing H_4DPP^{2+} (10 μM), $AcrH_2$ (20 mM), TsOH (30 mM), and PtNPs (0.16 mg mL^{-1}) under Ar at 298 K.

performed by adding additional amount of $AcrH_2$ and TsOH after 40 min photoirradiation. As a result, the same v_H values were obtained at least three times (Figure S6), ascertaining the robustness of this photocatalytic HER system. This result also suggests that the rate of photocatalytic HER depends on the concentration of $AcrH_2$ without decomposition of H_4DPP^{2+} and PtNPs. Surprisingly, the quantum yield (Φ) of photocatalytic HER was determined to be 17% at 710 nm, 12% at 480 nm, and 8% at 750 nm from the v_H values in Figure S7 by a photomultiplier and a comparative actinometer method (see Experimental Section). These Φ values at NIR regions are the highest ever reported in photocatalytic HER.

To gain a mechanistic insight into the photocatalytic HER, we performed nano-second laser flash photolysis (ns-LFP) in a mixed MeOH/MeCN solution (1:1, v/v). Upon photoexcitation at 532 nm to a deaerated MeOH/MeCN solution of H_4DPP^{2+} and TsOH, transient absorption spectra of H_4DPP^{2+} showed an absorption band at 560 nm at 0.8 μs after laser excitation. This indicates the formation of the triplet excited state of H_4DPP^{2+} ($^3(H_4DPP^{2+})^*$) that showed a μs-order lifetime ($\tau = 7.7$ μs) via intersystem crossing (ISC) from the singlet excited state of H_4DPP^{2+} ($^1(H_4DPP^{2+})^*$) (Figure S8).[26] Then, transient absorption spectra were measured in the presence of $AcrH_2$ to investigate photoinduced electron transfer (ET) from $AcrH_2$ to $^3(H_4DPP^{2+})^*$ (Figure 4a). The transient absorption spectrum changed to exhibit a new absorption band at 520 nm, which was ascribable to the formation of the one-electron reduced H_4DPP^{2+} ($H_4DPP^{\bullet+}$).[25,26] The decay time profile at 560 nm assigned to $^3(H_4DPP^{2+})^*$ coincided with the rise time profile at 520 nm due to $H_4DPP^{\bullet+}$ as shown in Figure 4b. The second-order rate constant (k_{et}) of photoinduced ET from $AcrH_2$ to $^3(H_4DPP^{2+})^*$ was determined to be 1.2×10^7 M^{-1} s^{-1} by changing [$AcrH_2$] (Figure S9). Judging from the lifetime of $^3(H_4DPP^{2+})^*$ and the determined k_{et} value, the saturation behavior of v_H in Figure 2a was well explained by a competitive manner between ET from $AcrH_2$ to $^3(H_4DPP^{2+})^*$ ($k_{et}[AcrH_2]$) and the decay of $^3(H_4DPP^{2+})^*$ ($1/\tau$) according to eq 2. The fitting line based on eq 2 is completely consistent with the saturation behavior in Figure 2a, indicating the rate-determining step in photocatalytic HER is the photoinduced ET from $AcrH_2$ to $^3(H_4DPP^{2+})^*$.

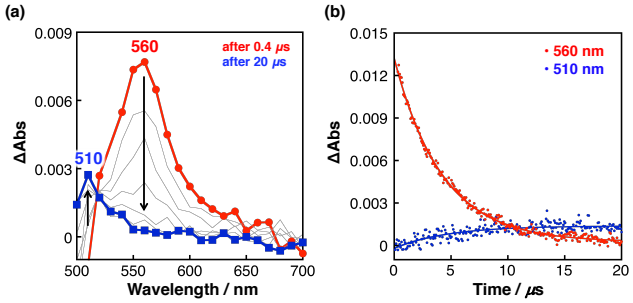

Figure 4. (a) Transient absorption spectra of H_4DPP^{2+} (40 μM) in the presence of $AcrH_2$ (12 mM) and TsOH (5 mM) in a deaerated MeOH/MeCN mixed solution (4 mL, 1:1 v/v) at 298 K taken at 0.4 μs (red) and 20 μs (blue) after nano-second laser excitation at 532 nm. (b) The decay and rise time profiles at 510 nm (blue) and 560 nm (red) in photoinduced ET from $AcrH_2$ to $^3(H_4DPP^{2+})^*$.

$$v_H = v_{max} \frac{k_{et}[AcrH_2]}{k_{et}[AcrH_2] + 1/\tau} \qquad (2)$$

The proposed HER mechanism is described in Figure 5. Upon photoexcitation of H_4DPP^{2+} in the presence of $AcrH_2$, photoinduced ET from $AcrH_2$ to $^3(H_4DPP^{2+})^*$ occurs to produce $H_4DPP^{\bullet+}$ as observed by ns-LFP. The fate of $AcrH_2^{\bullet+}$ was expected to form a radical species ($AcrH^\bullet$) *via* the deprotonation and the resulting $AcrH^\bullet$ species is capable of reducing another H_4DPP^{2+}.[25,34] Subsequent electron injection directly from $H_4DPP^{\bullet+}$ to PtNPs occurs to reduce a proton, affording a putative Pt-H species[31,32] on the surface of PtNPs, to evolve H_2 under catalytic conditions. Thus, we conclude that photoinduced ET from $AcrH_2$ to H_4DPP^{2+} and electron injection from $H_4DPP^{\bullet+}$ to PtNPs allows us to construct the efficient photocatalytic HER system by NIR irradiation.

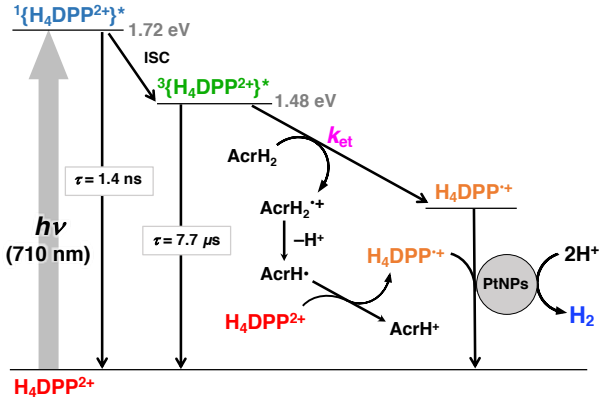

Figure 5. Proposed photocatalytic HER mechanism.

In conclusion, we have constructed NIR light-driven HER system composed of H_4DPP^{2+} and PtNPs showing the highest

quantum yield (Φ_{710} = 17%) ever reported. The HER mechanism was clarified on the basis of nano-second laser flash photolysis and dependence of the HER rates on concentrations of PtNPs, $AcrH_2$, and acids. The results presented herein are expected to contribute to the development of NIR light-driven HER by organic photocatalysts.

ASSOCIATED CONTENT

Supporting Information

Experimental details and kinetic data sets, including Figure S1-9.

AUTHOR INFORMATION

Corresponding Author

kojima@chem.tsukuba.ac.jp

Notes

The authors declare no competing financial interest.

ACKNOWLEDGMENTS

This work was supported by a Grant-in-Aid (17H03027) from the Japan Society of Promotion of Science (JSPS, MEXT) of Japan. Financial support through CREST (JST) is also appreciated (JPMJCR16P1).

REFERENCES

(1) *Innovation, Markets and Sustainable Energy: The Challenge of Hydrogen and Fuel Cells*; Pogutz, S., Russo, A., Migliavacca, P., Eds.; Edward Elgar: Cheltenham, UK; Northampton, MA, 2009.

(2) Armaroli, N.; Balzani, V. The Hydrogen Issue. *ChemSusChem.* **2011**, *4*, 21-36.

(3) Esswein, M. J.; Nocera, D. G. Hydrogen Production by Molecular Photocatalysis. *Chem. Rev.* **2007**, *107*, 4022–4047.

(4) Teets, T. S.; Nocera, D. G. Photocatalytic Hydrogen Production. *Chem. Commun.* **2011**, *47*, 9268-9274.

(5) Dempsey, J. L.; Brunschwig, B. S.; Winkler, J. R.; Gray, H. B. Hydrogen Evolution Catalyzed by Cobaloximes. *Acc. Chem. Res.* **2009**, *42*, 1995-2004.

(6) Han, Z.; Eisenberg, R. Fuel from Water: The Photochemical Generation of Hydrogen from Water. *Acc. Chem. Res.* **2014**, *47*, 2537-2544.

(7) Fukuzumi, S.; Lee, Y.-M.; Nam, W. Thermal and Photocatalytic Production of Hydrogen with Earth-Abundant Metal Complexes. *Coord. Chem. Rev.* **2018**, *355*, 54-73.

(8) Kaeffer, N.; Chavarot-Kerlidou, M.; Artero, V. Hydrogen Evolution Catalyzed by Cobalt Diimine–Dioxime Complexes. *Acc. Chem. Res.* **2015**, *48*, 1286-1295.

(9) Zhu, H.; Song, N.; Lv, H.; Hill, C. L.; Lian, T. Near Unity Quantum Yield of Light-Driven Redox Mediator Reduction and Efficient H_2 Generation Using Colloidal Nanorod Heterostructures. *J. Am. Chem. Soc.* **2012**, *134*, 11701-11708.

(10) Li, X.-B.; Gao, Y.-J.; Wang, Y.; Zhan, F.; Zhang, X.-Y.; Kong, Q.-Y.; Zhao, N.-J.; Guo, Q.; Wu, H.-L.; Li, Z.-J.; Tao, Y.; Zhang, J.-P.; Chen, B.; Tung, C.-H.; Wu, L.-Z. Self-Assembled Framework Enhances Electronic Communication of Ultrasmall-Sized Nanoparticles for Exceptional Solar Hydrogen Evolution. *J. Am. Chem. Soc.* **2017**, *139*, 4789–4796.

(11) Zhu, M.; Cai, X.; Fujitsuka, M.; Zhang, J.; Majima, T. $Au/La_2Ti_2O_7$ Nanostructures Sensitized with Black Phosphorus for Plasmon-Enhanced Photocatalytic Hydrogen Production in Visible and Near-Infrared Light. *Angew. Chem. Int. Ed.* **2017**, *56*, 2064-2068.

(12) Lian, Z.; Sakamoto, M.; Vequizo, J. J. M.; Ranasinghe, C. S. K.; Yamakata, A.; Nagai, T.; Kimoto, K.; Kobayashi, Y.; Tamai, N.; Teranishi, T. Plasmonic p–n Junction for Infrared Light to Chemical Energy Conversion. *J. Am. Chem. Soc.* **2018**, *141*, 2446-2450.

(13) Rousset, E.; Chartrand, D.; Ciofini, I.; Marvaud, V.; Hanan, G. S. Red-Light-Driven Photocatalytic Hydrogen Evolution Using a Ruthenium Quaterpyridine Complex. *Chem. Commun.* **2015**, *51*, 9261-9264.

(14) Tsuji, Y.; Yamamoto, K.; Yamauchi, K.; Sakai, K. Near-Infrared Light-Driven Hydrogen Evolution from Water Using a Polypyridyl Triruthenium Photosensitizer. *Angew. Chem. Int. Ed.* **2017**, *57*, 208-212.

(15) Sayre, H. J.; Millet, A.; Dunbar, K. R.; Turro, C. Photocatalytic H_2 production by Dirhodium(II,II) Photosensitizers with Red Light. *Chem. Commun.* **2018**, *54*, 8332-8334.

(16) Whittemore, T. J.; Xue, C.; Huang, J.; Gallucci, J. C.; Turro, C. Single-Chromophore Single-Molecule Photocatalyst for the Production of Dihydrogen Using Low-Energy Light. *Nat. Chem.* **2020**, *12*, 180-185.

(17) Dolphin, D. *The Porphyrins V3 & V5*, Academic Press, New York, 1978.

(18) Ladomenou, K.; Natali, M.; Iengo, E.; Charalampidis, G.; Scandola, F.; Coutsolelos, A. G. Photochemical Hydrogen Generation with Porphyrin-Based Systems. *Coord. Chem. Rev.* **2015**, *304-305*, 38-54.

(19) Hasobe, T.; Sakai, H.; Mase, K.; Ohkubo, K.; Fukuzumi, S. Remarkable Enhancement of Photocatalytic Hydrogen Evolution Efficiency Utilizing an Internal Cavity of Supramolecular Porphyrin Hexagonal Nanocylinders Under Visible-Light Irradiation. *J. Phys. Chem. C* **2013**, *117*, 4441-4449.

(20) Sternberg, E. D.; Dolphin, D.; Brückner, C. Porphyrin-Based Photosensitizers for Use in Photodynamic Therapy. *Tetrahedron* **1998**, *54*, 4151-4202.

(21) Lash, T. D.; Chandrasekar, P. Synthesis of Tetraphenyltetraacenaphthoporphyrin: A New Highly Conjugated Porphyrin System with Remarkably Red-Shifted Electronic Absorption Spectra. *J. Am. Chem. Soc.* **1996**, *118*, 8767-8768.

(22) Röder, B.; Büchner, M.; Rückmann, I.; Senge, M. O. Correlation of Photophysical Parameters with Macrocycle Distortion in Porphyrins with Graded Degree of Saddle Distortion. *Photochem. Photobiol. Sci.* **2010**, *9*, 1152-1158.

(23) Medforth, C. J; Senge, M. O.; Smith, K. M.; Sparks, L. D.; Shelnutt, J. A. Nonplanar Distortion Modes for Highly Substituted Porphyrins. *J. Am. Chem. Soc.* **1992**, *114*, 9859-9869.

(24) Ishizuka, T.; Ohkawa, S.; Ochiai, H.; Hashimoto, M.; Ohkubo, K.; Kotani, H.; Sadakane, M.; Fukuzumi, S.; Kojima, T. A Supramolecular Photocatalyst Composed of a

Polyoxometalate and a Photosensitizing Water-Soluble Porphyrin Diacid for the Oxidation of Organic Substrates in Water. *Green Chem.* **2018**, *20*, 1975-1980.

(25) Aoki, E.; Suzuki. W.; Kotani, H.; Ishizuka, T.; Sakai, H.; Hasobe, T.; Kojima, T. Efficient Photocatalytic Proton-Coupled Electron-Transfer Reduction of O_2 by a Saddle-Distorted Porphyrin as a Photocatalyst. *Chem. Commun.* **2019**, *55*, 4925-4928.

(26) Nakanishi, T.; Ohkubo, K.; Kojima, T.; Fukuzumi, S. Reorganization Energies of Diprotonated and Saddle-Distorted Porphyrins in Photoinduced Electron-Transfer Reduction Controlled by Conformational Distortion. *J. Am. Chem. Soc.* **2009**, *131*, 577-584.

(27) Fukuzumi, S.; Honda, T.; Kojima, T. Structures and Photoinduced Electron Transfer of Protonated Complexes of Porphyrins and Metallophthalocyanines. *Coord. Chem. Rev.* **2012**, *256*, 2488-2502.

(28) Kielmann, M.; Senge, M. O. Molecular Engineering of Free-Base Porphyrins as Ligands–The N-H•••X Binding Motif in Tetrapyrroles. *Angew. Chem. Int. Ed.* **2019**, *58*, 418-441.

(29) Suzuki, W.; Kotani, H.; Ishizuka, T.; Kojima, T. Dioxygen/Hydrogen Peroxide Interconversion Using Redox Couples of Saddle-Distorted Porphyrins and Isophlorins. *J. Am. Chem. Soc.* **2019**, *141*, 5987-5994.

(30) Wang, H.; Wang, Y.; Zhu, Z.; Sapi, A.; An, K.; Kennedy, G.; Michalak, W. D.; Somorjai, G. A. Influence of Size-Induced Oxidation State of Platinum Nanoparticles on Selectivity and Activity in Catalytic Methanol Oxidation in the Gas Phase. *Nano Lett.* **2013**, *13*, 2976-2979.

(31) Kotani, H.; Hanazaki, R.; Ohkubo, K.; Yamada, Y.; Fukuzumi, S. Size- and Shape-Dependent Activity of Metal Nanoparticles as Hydrogen-Evolution Catalysts: Mechanistic Insights into Photocatalytic Hydrogen Evolution. *Chem.-Eur. J.* **2011**, *17*, 2777-2785.

(32) Zhou, M.; Bao, S.; Bard, A. J. Probing Size and Substrate Effects on the Hydrogen Evolution Reaction by Single Isolated Pt Atoms, Atomic Clusters, and Nanoparticles. *J. Am. Chem. Soc.* **2019**, *141*, 7327-7332.

(33) Under catalytic conditions employed in this study, H_2DPP is completely diprotonated by acids used to be H_4DPP^{2+}. See: Suzuki, W.; Kotani, H.; Ishizuka, T.; Shiota, Y. Yoshizawa, K.; Kojima, T. Formation of Supramolecular Hetero-Triads by Controlling the Hydrogen Bonding of Conjugate Bases with a Diprotonated Porphyrin Based on Electrostatic Interaction. *Chem. Commun.* **2017**, *53*, 6359-6362.

(34) Fukuzumi, S.; Tokuda, Y.; Kitano, T.; Okamoto, T.; Otera, J. Electron-Transfer Oxidation of 9-Substituted 10-Methyl-9,10-Dihydroacridines. Cleavage of the Carbon-Hydrogen vs. Carbon-Carbon Bond of the Radical Cations. *J. Am. Chem. Soc.* **1993**, *115*, 8960-8968.

Insert Table of Contents artwork here